Periodic Changes in Radius, Temperature, and Luminosity in the Pulsation of HADS-Type Variable Stars V451 Draconis, NP Lyncis, V460 Andromedae, V417 Bootis, and 2MASS J01462408+4913115

Moyuru Nakamori
Hiroshima International School, Hiroshima City, Hiroshima Prefecture, Japan; moyuruseal0321@gmail.com

Yuno Kondo
Fuji Sacred Heart School, Susono City, Shizuoka Prefecture, Japan; ykss05300125@gmail.com

Yumeto Yamada
Ibaraki High School, Mito City, Ibaraki Prefecture, Japan; megane.beans132109@gmail.com

Satsuki Abe
Morioka Daisan High School, Morioka City, Iwate Prefecture, Japan; satsukiazalea0517@gmail.com

Received May 6, 2026; revised June 23, July 18, 2026; accepted July 20, 2026

Abstract We investigated the phase-dependent relationships among luminosity, temperature, and radius in select High-Amplitude δ Scuti (HADS-type) variable stars using archived photometric data from the Zwicky Transient Facility (ZTF). Light curves were phase-folded, effective temperatures were estimated from color indices, and stellar radii were derived assuming blackbody radiation. The analysis showed that stars with similar luminosity amplitudes exhibited different temperature and radius variations, suggesting that luminosity changes do not uniquely determine the underlying physical variations.

1. Introduction

Pulsating variable stars exhibit periodic changes in luminosity driven by variations in their internal structure. In particular, High-Amplitude δ Scuti (HADS-type) stars show large-amplitude radial pulsations that produce observable changes in brightness, temperature, and radius over short timescales. HADS-type stars typically exhibit brightness variations of about 0.3–0.8 mag and short pulsation periods of about 0.03–0.3 day, and are predominantly radial pulsators (Breger 2000, 2007).

In this study, we selected five HADS-type stars based on the availability of multi-band light curve data and the regularity of their periodic variability, both of which are necessary for phase-folding and phase-dependent analysis using archived photometric data from the Zwicky Transient Facility (Zwicky Transient Facility 2025).Those stars are V451 Draconis, NP Lyncis, V460 Andromedae, V417 Bootis, and 2MASS J01462408+4913115.

This study examines whether stars with similar luminosity amplitudes show similar temperature and radius variations. Table 1 shows details of the stars examined in this study.

1.1. Previous works

V451 Dra has been included in recent TESS-based work on HADS stars. Xue *et al.* (2023) classified it as a single-mode HADS and listed a period of 0.05581 day with a TESS amplitude of 169.4 mmag. This supports the use of V451 Dra as a relatively regular short-period HADS target in the present analysis.

NP Lyn appears to have more limited star-specific literature. Its basic classification and pulsation period are available through variable-star catalogs, but detailed studies of its phase-dependent temperature and radius behavior appear to be limited.

Table 1. Properties of the five HADS-type variable stars.

Star	*Period (days)*	*Distance (pc)*	*Mean g (mag)*	*g amplitude (mag)*	*Mean g − r*	$T_{eff,GSP}$ *(K)*	$[M/H]_{GSP}$	A_0 *(mag)*
V451 Dra	0.05581096	1055 ± 19	12.94 ± 0.01	0.73 ± 0.02	0.04 ± 0.02	7477	–0.98	0.036
NP Lyn	0.067751	1616 ± 49	13.25 ± 0.01	0.77 ± 0.02	0.09 ± 0.02	6969	–1.54	0.017
V460 And	0.07498076	1557 ± 58	13.19 ± 0.01	0.85 ± 0.02	0.05 ± 0.02	11993	–0.89	1.179
V417 Boo	0.08664937	1815 ± 79	13.20 ± 0.01	0.59 ± 0.02	0.06 ± 0.02	7394	–0.85	0.005
2MASS J01462408+4913115	0.1060238	2677 ± 177	14.36 ± 0.01	0.73 ± 0.02	0.20 ± 0.02	7146	–0.90	0.547

Note: Periods and HADS classifications were obtained from AAVSO (2026). Targets showing no evidence of additional pulsation modes in the phase-folded light curves were selected to minimize interference from multiperiodicity. Distances were derived from Gaia parallaxes through SIMBAD, and color indices were obtained from SIMBAD. The Teff, GSP, [M/H] GSP, and A0 values are Gaia GSP-Phot catalog estimates. The monochromatic A0 values were not applied directly to the ZTF passbands. All other data were obtained from the ZTF archive.

Therefore, NP Lyn is useful in this study as a catalogued HADS target for which the same analysis pipeline can be applied consistently with the other stars.

V460 And has been examined spectroscopically in the LAMOST δ Scuti sample. Qian *et al.* (2018) listed V460 And with a period of 0.074981 day, spectral type A6, T_{eff} = 8120 K, log g = 4.16, and [Fe/H] = –0.25, while the AAVSO International Variable Star Index (VSX; Watson *et al.* 2014) lists a spectral type of F5 and classifies the object as HADS. These values provide external comparison points for the photometric temperature estimates in this study. The Gaia GSP-Phot temperature of 11,993 K listed in Table 1 is substantially higher than both the LAMOST value and the phase-dependent estimates derived below. Because the Gaia temperature and extinction are inferred together from the same catalog pipeline, the Gaia temperature is treated cautiously rather than adopted as the physical temperature of V460 And (Gaia Collab. 2023).

V417 Boo has received more detailed individual study than the other targets. Alton and Gilchrist (2022) performed CCD (B)- and (V)-band photometry, discrete Fourier transformation, period analysis, and evolutionary modeling. Their analysis found a fundamental oscillation frequency near 11.5408 cycles per day, with harmonics up to $4f_0$, but no other statistically significant independent frequencies after pre-whitening. They concluded that V417 Boo is likely a monoperiodic radial pulsator and found no substantive change in the fundamental period or (V)-band amplitude over the previous 11 years. This makes V417 Boo especially useful for comparison because its pulsation behavior has already been studied in detail.

For 2MASS J01462408+4913115, previous work appears to be mainly catalog-based, and detailed star-specific studies were not found. Its inclusion therefore allows the present study to extend the same phase-dependent temperature and radius analysis to a less-studied HADS-type target. Overall, previous work provides classifications, periods, amplitudes, and some spectroscopic or evolutionary information for several of the targets, but detailed comparisons of phase-dependent temperature and radius behavior across these five stars remain limited.

2. Research methods

This study was conducted using archived photometric data from the Zwicky Transient Facility (ZTF) database (Zwicky Transient Facility 2025). Five HADS-type variable stars were selected: V451 Dra, NP Lyn, V460 And, V417 Boo, and 2MASS J01462408+4913115. Time-series measured apparent magnitudes in the g, r, and i bands were obtained for each object and used to construct phase-folded light curves.

Because observations are not uniformly spaced in time, the data were phase-folded using the variability period. The phase was defined such that phase 0 corresponds to the minimum brightness in the g-band, allowing consistent alignment across all objects. The g-band was selected as the reference band because it is the band with the most available data. This enables direct comparison across stars by preserving the phase separation between minimum and maximum brightness after rephasing.

To analyze the periodic variability, each light curve was modeled using a Fourier series. The number of harmonic terms was selected separately for each star and band to avoid overfitting while still providing a smooth and continuous representation of brightness as a function of phase.

2.1. Temperature estimation

The ZTF photometric data were converted from the SDSS-like system to the Johnson-Cousins photometric system using transformation equations based on Jordi *et al.* (2006). The equations used here are:

$$V - R_C = \frac{(g - r) + 0.139}{1.646}, \qquad (1)$$

$$V - I_C = \frac{(g - i) + 0.36}{1.481}, \qquad (2)$$

From the transformed magnitudes, the color indices $V - R_C$ and $V - I_C$ were calculated. These were used to estimate the effective temperature T_{eff} using empirically calibrated color-temperature relations based on the infrared flux method (IRFM) (Casagrande *et al.* 2010).

Following Casagrande *et al.* (2010), the calibration is expressed as

$$\theta_{eff} = a_0 + a_1 X + a_2 X^2 + a_3 X\,[M/H] + a_4\,[M/H] + a_5\,[M/H]^2, \qquad (3)$$

where

$$\theta_{eff} = \frac{5040}{T_{eff}}, \qquad (4)$$

The effective temperature is then obtained as

$$T_{eff} = \frac{5040}{\theta_{eff}}, \qquad (5)$$

Gaia DR3 metallicity estimates, $[M/H]_{GSP}$, were used as first-order proxies for the metallicity term in the color-temperature calibration. This was done because the relation of Casagrande *et al.* (2010) includes a metallicity dependence, and assuming solar metallicity for all targets would introduce an unnecessary systematic offset. The use of Gaia $[M/H]_{GSP}$ is treated as an approximation because it is a catalog-level stellar parameter rather than a phase-resolved measurement.

Substituting the coefficients obtained from Casagrande *et al.* (2010), the formulae become:

$$\theta_{eff,V-R_C} = a_0 + a_1 (V - R_C) + a_2 (V - R_C)^2 + a_3 (V - R_C)\,[M/H] + a_4\,[M/H] + a_5\,[M/H]^2\,. \qquad (6)$$

and

$$\theta_{eff,V-I_C} = a_0 + a_1 (V - I_C) + a_2 (V - I_C)^2 + a_3 (V - I_C)\,[M/H] + a_4\,[M/H] + a_5\,[M/H]^2\,. \qquad (7)$$

Temperature estimates were calculated independently from $V-R_C$ and $V-I_C$, and the results were averaged to reduce systematic uncertainty.

2.2. Derivation of radius from photometric data

The apparent magnitude is related to the observed flux by Pogson's equation:

$$m_\nu = -2.5 \log_{10}\left(\frac{f_\nu}{f_{\nu,0}}\right). \tag{8}$$

Rearranging, the flux is given by:

$$f_\nu = F_{\nu,0^{10}-0.4m_\nu}. \tag{9}$$

The observed flux f_ν and the stellar surface flux F_ν are related by:

$$f_\nu = F_\nu \frac{R^2}{d^2}. \tag{10}$$

Assuming isotropic radiation, the surface flux is related to the specific intensity by:

$$F_\nu = \pi B_\nu (T_{eff}), \tag{11}$$

where $B_\nu (T_{eff})$ is given by Planck's law:

$$B_\nu (T_{eff}) = \frac{2h\nu^3}{c^2 (e^{h\nu/(kT_{eff})} - 1)}. \tag{12}$$

Combining these relations gives:

$$R = d\sqrt{\frac{f_\nu}{F_\nu}}, \tag{13}$$

Substituting for f_ν and F_ν, we obtain:

$$R = d\sqrt{\frac{f_{\nu,0}10^{-0.4m_\nu}}{\pi B_\nu(T_{eff})}}, \tag{14}$$

Equivalently, using Planck's law explicitly,

$$R = d\sqrt{\frac{f_{\nu,0}10^{-0.4m_\nu} c^2 (e^{h\nu/(kT_{eff})} - 1)}{2\pi h\nu^3}}, \tag{15}$$

Here, the distance was calculated using the formula

$$d = \frac{1}{p}, \tag{16}$$

where p represents the parallax of the star obtained from the Gaia database (Gaia Collab. 2023).

2.3. Final analysis

The phase-dependent temperature and radius were plotted alongside the light curve. By comparing these quantities in phase space, we analyzed their relative variation and phase relationships throughout the pulsation cycle.

In this analysis, we assumed isotropic emission. Furthermore, we did not consider the effects of interstellar extinction. Uncertainties arise primarily from photometric errors, transformation relations, and temperature calibration, and propagate into the derived radius values.

Gaia A_0 is a monochromatic catalog parameter rather than an extinction value in the ZTF g, r, or i passband. An extinction correction would require converting A_0 to the ZTF passbands using an adopted extinction law and passband-specific coefficients, or using an independent reddening estimate. An exploratory correction based on the Gaia catalog solution for V460 And moved the transformed colors outside the applicable range of the adopted color-temperature calibration. That correction was therefore not adopted.

A validity test that was performed consisted of inputting data for the Sun, and comparing the output value from this process to the literature value. This returned data that included the literature value of the Sun in its uncertainty range, so the pipeline for finding the physical values can be considered as valid.

2.4. Model assumptions

In this analysis, the stellar emission was approximated as blackbody radiation when relating flux and temperature. This implies that the effective temperature, T_{eff}, derived from color-temperature relations is treated as equivalent to the blackbody temperature used in Planck's law.

Although real stellar spectra deviate from ideal blackbody radiation due to atmospheric absorption and emission features, this approximation is commonly used when deriving bulk stellar properties such as radius. Therefore, it provides a reasonable first-order estimate for the phase-dependent variation of stellar radius.

3. Uncertainties

The uncertainties were propagated according to the standard uncertainty propagation model. An example of this propagation method would be the calculation of flux from the magnitude. The formula used to calculate the uncertainty is:

$$\Delta f_\nu = 0.4 \ln(10) f_\nu \Delta m_\nu. \tag{17}$$

The sources of uncertainty were ZTF archival data, the SDSS-Johnson conversion formula, the temperature estimation formula, and Gaia distance data. For addition, the absolute uncertainties were added in quadrature and for multiplication and division, the fractional uncertainties were added in quadrature. As a result, the percentage uncertainty of the temperature ranged from 1.5% to 3.9% depending on the star. The percentage uncertainty of the radius ranged from 2.7% to 4.7%.

4. Results

4.1. Light curves

In the following five figures, the green dots represent the g-band data, the red dots represent the r-band data, and the orange dots represent the i-band data. They are observed phase-

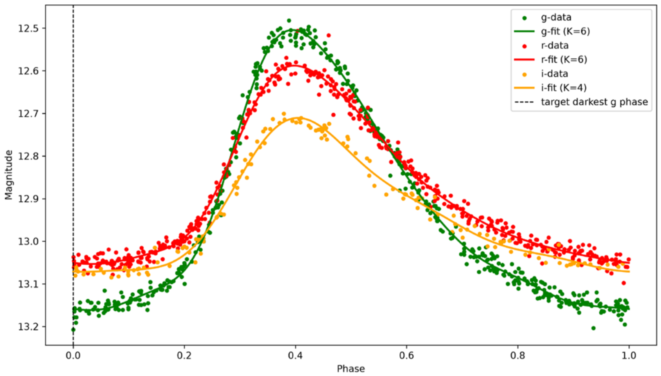

Figure 1. Phase-folded g-, r-, and i-band light curves for V451 Dra.

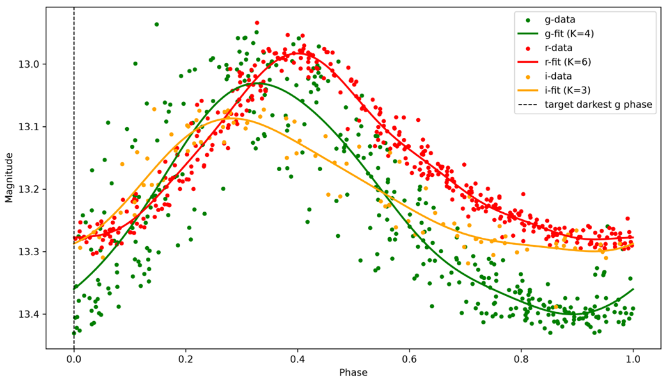

Figure 2. Phase-folded g-, r-, and i-band light curves for NP Lyn.

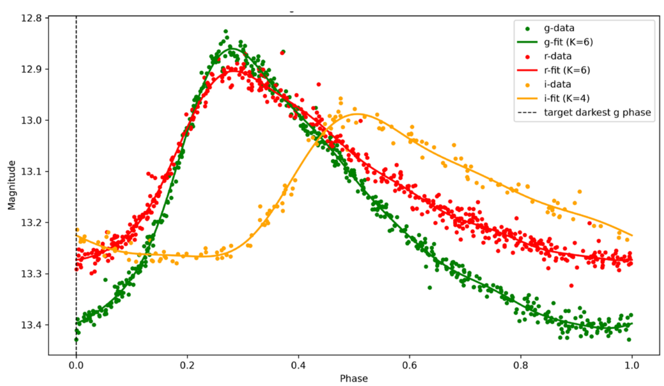

Figure 3. Phase-folded g-, r-, and i-band light curves for V460 And.

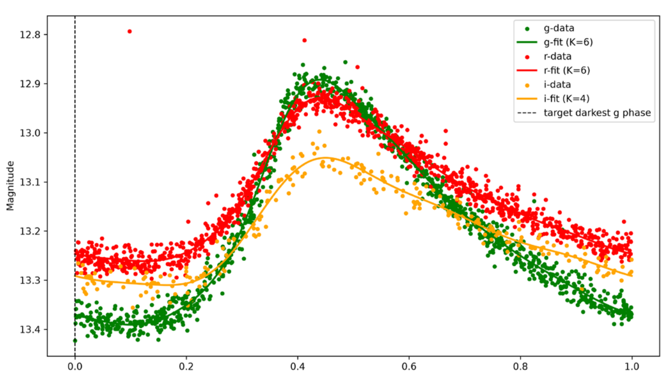

Figure 4. Phase-folded g-, r-, and i-band light curves for V417 Boo.

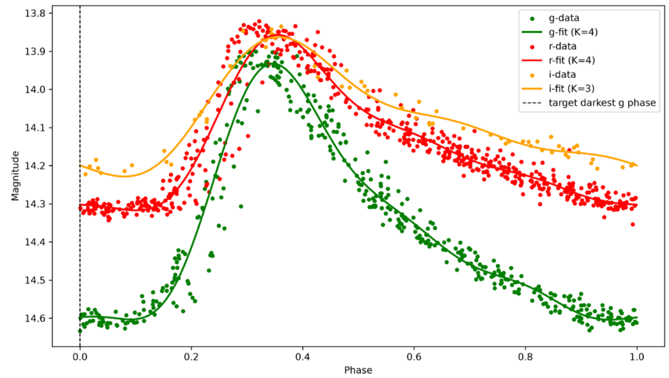

Figure 5. Phase-folded g-, r-, and i-band light curves for 2MASS J01462408+4913115.

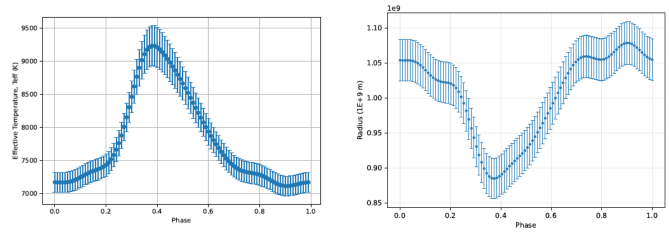

Figure 6: Phase-folded effective temperature (left) and stellar radius (right) curves for V451 Dra.

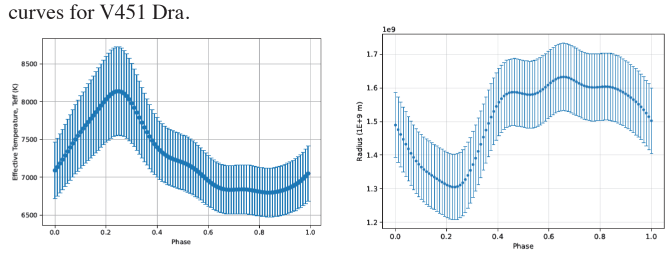

Figure 7. Phase-folded effective temperature (left) and stellar radius (right) curves for NP Lyn.

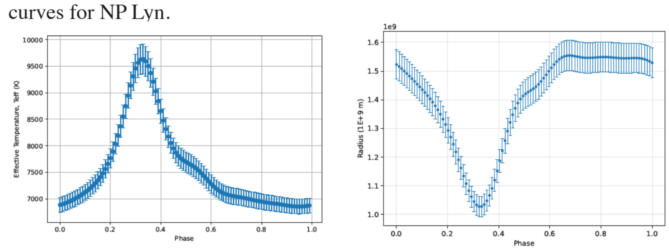

Figure 8. Phase-folded effective temperature (left) and stellar radius (right) curves for V460 And.

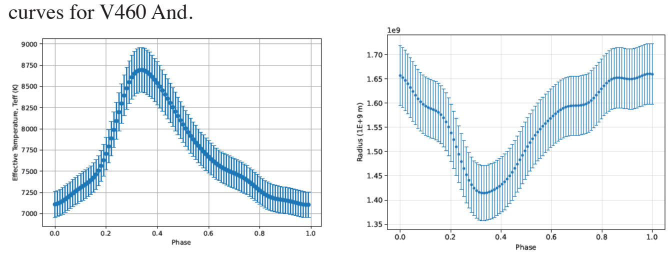

Figure 9. Phase-folded effective temperature (left) and stellar radius (right) curves for V417 Boo.

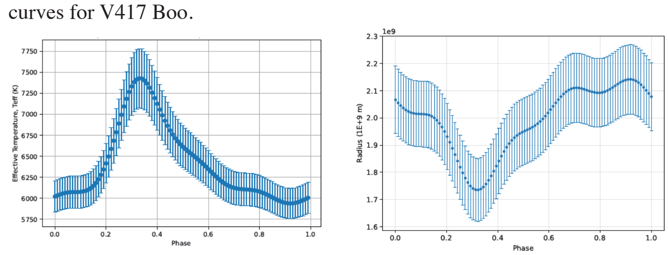

Figure 10. Phase-folded effective temperature (left) and stellar radius (right) curves for 2MASS J01462408+4913115.

folded data and are not corrected for interstellar reddening. The horizontal axis is the folded phase from 0 to 1, and the vertical axis represents the apparent magnitude from the ZTF archive. The green, red, and orange lines represent the Fourier fitted lines. The black dotted vertical line represents phase 0.0.

4.2. Temperature and radius curves

The horizontal axis represents the pulsation phase (0–1), aligned such that phase 0 corresponds to the minimum brightness in the g-band. The curves show temperature and radius values calculated from photometric data at each phase, with vertical error bars indicating propagated uncertainties. The effective temperature is estimated from color indices using empirically calibrated color-temperature relations (Casagrande *et al.* 2010), and the radius is derived from flux relations under the assumption of blackbody radiation.

Figures 1 through 5 show the light curve, while Figures 6 to 10 show the temperature curve and the radius curve of the HADS-type variable stars investigated in this study. This was found using the procedures described in section 2. This allows the rates of change in radius and temperature to be examined across both bright and faint phases.

For V460 And, the temperatures derived separately from $V – R_C$ and $V – I_C$ both reached their maxima at phase 0.33. The $V – R_C$ estimate ranged from 7,614 K to 9,954 K, giving $T_{max}/T_{min} = 1.31$, whereas the $V – I_C$ estimate ranged from 6,071 K to 9,317 K, giving $T_{max}/T_{min} = 1.53$. Their adopted mean ranged from 6,853 K to 9,635 K and gave the ratio 1.41 reported in Table 3. Thus, the phase of maximum temperature is unchanged by the displaced i-band curve, but the amplitude and phase of minimum temperature are sensitive to the selected color index.

As shown in Table 2, the temperature curve reaches a maximum and the radius curve reaches a minimum at approximately the same phase. This inverse phase relationship is expected, and aids in the verification of the methodology. All stars showed the same predicted trend: the temperature was highest and the radius was smallest at maximum brightness.

However, there seems to be a consistent lag between the maximum of the radius and the minimum of the temperature, and the minimum of the g-band brightness.

5. Discussion

In pulsating variable stars, changes in observed brightness can arise from different combinations of temperature and radius variation. The results of this study show that there is not a single one-to-one relationship between light curve amplitude, luminosity variation, temperature change, and radius change.

For example, 2MASS J01462408+4913115 and V417 Boo show similar luminosity increases of approximately 1.60×. These two stars also show relatively similar temperature and radius ratios, suggesting that similar luminosity variations can sometimes correspond to similar physical changes. However, this pattern is not universal. V460 And also shows a comparable luminosity increase, but it has a much larger temperature increase and a stronger decrease in radius than either 2MASS J01462408+4913115 or V417 Boo. This indicates that a similar luminosity ratio does not necessarily imply the same balance between temperature and radius variation. Moreover, comparing the values in Tables 1 and 2, it can be suggested that the variation in luminosity does not necessarily correlate with the g-band amplitude.

For V460 And, the separate $V – R_C$ and $V – I_C$ temperature estimates both reach maximum temperature at phase 0.33. Their temperature ratios are 1.31 and 1.53, respectively, compared with 1.41 for their adopted mean. Thus, the phase of maximum temperature is unchanged by the displaced i-band curve, although the inferred temperature amplitude depends on the selected color index.

A similar disparity appears when comparing V451 Dra and 2MASS J01462408+4913115. These stars have nearly the same (g)-band amplitude in the raw light curve data, but their derived luminosity, temperature, and radius ratios are not identical. This suggests that a similar apparent brightness amplitude does not necessarily produce the same inferred physical variation.

To examine whether metallicity may be related to these differences, exploratory correlations were calculated between the Gaia $[M/H]_{GSP}$ values and the luminosity, temperature, and radius ratios in Table 3, as well as the phase of minimum temperature in Table 2. No clear correlation was found between metallicity and any of the three ratios. The phase of minimum temperature increased monotonically with metallicity across the five targets (Spearman $\rho = 1.00$, exact permutation $p = 0.017$), but this result did not remain below $p = 0.05$ after a Bonferroni correction for the four comparisons (adjusted $p = 0.067$). Given the small sample and the approximate catalog-level metallicities, this pattern is treated as exploratory and no physical dependence on metallicity is claimed. Other factors, including color, period, and evolutionary state, may also influence the relative temperature and radius contributions to luminosity.

Table 2. Points of maximum and minimum luminosity, temperature, and radius.

Star	φ (g_{max})	φ (g_{min})	φ (T_{max})	φ (T_{min})	φ (R_{max})	φ (R_{min})
V451 Dra	0.37	0.00	0.37	0.90	0.89	0.35
NP Lyn	0.34	0.00	0.25	0.84	0.65	0.23
V460 And	0.33	0.00	0.33	0.95	0.67	0.32
V417 Boo	0.44	0.00	0.34	0.98	0.98	0.33
2MASS J01462408+4913115	0.30	0.00	0.33	0.92	0.91	0.32

Note: All phases are rounded to 0.01.

Table 3. Ratios of maximum to minimum luminosity, temperature, and radius.

Star	L_{max}/L_{min}	T_{max}/T_{min}	R_{min}/R_{max}
V451 Dra	1.92	1.30	0.82
NP Lyn	1.33	1.20	0.80
V460 And	1.72	1.41	0.66
V417 Boo	1.60	1.22	0.85
2MASS J01462408+4913115	1.60	1.25	0.81

Note: Change describes the ratio between the maximum and minimum value.

The low catalog metallicities raise the question of whether some targets could be related to the metal-poor SX Phoenicis population. Nevertheless, all five objects are catalogued by AAVSO VSX as HADS stars, and Gaia GSP-Phot metallicities alone are insufficient to establish a population-based reclassification. Spectroscopic abundances and full kinematic information would be required to distinguish this possibility. The HADS classifications are therefore retained in this study.

Overall, these comparisons indicate that HADS-type stars can reach similar luminosity changes through different temperature and radius behavior. In some cases, similar luminosity ratios are associated with similar temperature and radius ratios, while in other cases they are not. Therefore, the relationship between brightness variation and the underlying physical pulsation is not unique across the five stars examined in this study.

6. Conclusion

Based on observations of the five selected HADS-type stars, all targets showed the expected phase behavior: the effective temperature reached a maximum and the derived radius reached a minimum near maximum brightness. Within a phase resolution of 0.01, no clear lag was observed between maximum temperature and minimum radius.

The results in Table 3 also show that similar luminosity ratios do not necessarily correspond to similar temperature and radius ratios. In particular, V460 And and V417 Boo had similar luminosity ratios, but showed different temperature and radius variations. This suggests that individual HADS-type stars may differ in how luminosity variation is produced through changes in temperature and radius.

7. Evaluation and future extensions

Although this study examined the process of pulsation in HADS-type stars, it is important to point out that this process contains several limitations.

First, the calibration from Casagrande *et al.* (2010) is mainly targeted for stars of spectral type F, G, and K. The HADS-type stars we examined in this process are mainly early-type F and late-type A stars, which are slightly earlier than the target of Casagrande *et al.* (2010).

Another limitation is the lack of a reliable interstellar-reddening correction. Extinction changes both the color indices used for temperature and the flux used for radius, so it can bias the absolute temperature and radius. The especially large Gaia catalog value for V460 And, A_0 =1.179 mag, cannot be applied directly to the ZTF bands because A_0 is monochromatic and is inferred jointly with the Gaia GSP-Phot temperature. As described in section 2.3, an exploratory correction moved the colors outside the applicable calibration range, so it was rejected rather than incorporated into the final values. Future work should use an independent three-dimensional dust map or spectroscopic reddening estimate together with passband-specific extinction coefficients and a temperature calibration valid for the resulting intrinsic colors.

Because interstellar extinction is effectively constant over a pulsation cycle, it is not expected to change the observed phase of a single-band light curve extremum. Nevertheless, the nonlinear color–temperature and Planck relations mean that extinction can affect temperature and radius amplitudes and ratios even when it is phase-independent. The phase relationships are therefore more robust than the absolute values and amplitude ratios.

As an extension, future work should investigate how metallicity (Astronomical Society of Japan 2025), spectral type, radius, and temperature influence the amplitudes and phase relationships of these variations. This work may necessitate the use of other forms of archival data, as there was not enough data in the ZTF archive to clearly analyze those factors.

8. Acknowledgements

We express our sincere gratitude to all those involved in this research, including professors, staff at the Sendai Astronomical Observatory, the analysis team, and the SLA team, led by Mr. Hirotaka Matsumiya in Tohoku University, for their valuable advice and guidance throughout the study.

References

Alton, K. B., and Gilchrist, W. A. Jr. 2022, *J. Amer. Assoc. Var. Star Obs.*, **50**, 61.

Astronomical Society of Japan. 2025, Astronomical dictionary (https://astro-dic.jp).

Breger, M. 2000, in *Delta Scuti and Related Stars*, ASP Conf. Ser. 210, eds. M. Breger, M. Montgomery, Astronomical Society of the Pacific, San Francisco, 3.

Breger, M. 2007, *Commun. Asteroseismology*, **150**, 25.

Casagrande, L., Ramirez, I., Melendez, J., Bessell, M., and Asplund, M. 2010, *Astron. Astrophys.*, **512A**, 54.

Gaia Collaboration. 2023, Astron. Astrophys., 674A, 1.

Jordi, K., Grebel, E. K., and Ammon, K. 2006, *Astron. Astrophys.*, **460**, 339.

Qian, S.-B., Li, L.-J., He, J.-J., Zhang, J., Zhu, L.-Y., and Han, Z.-T. 2018, *Mon. Not. Roy. Astron. Soc.*, **475**, 478.

Watson, C., Henden, A. A., and Price, A. 2014, AAVSO International Variable Star Index VSX (Watson+, 2006–2014; https://vsx.aavso.org).

Xue, W., Niu, J.-S., Xue, H.-F., and Yin, S. 2023, *Res. Astron. Astrophys.*, **23**, 075002.

Zwicky Transient Facility. 2025 Zwicky transient facility (ZTF; https://irsa.ipac.caltech.edu/Missions/ztf.html).